Article

How Solid-Electrolyte-Interphase Forms in Aqueous Electrolytes

Liumin Suo, Dahyun Oh, yuxiao lin, Zengqing Zhuo, Oleg Borodin, Tao Gao, fei wang, Akihiro Kushima, Ziqiang Wang, Ho-Cheol Kim, Yue Qi, Wanli Yang, Feng Pan, Ju Li, kang xu, and Chunsheng Wang

J. Am. Chem. Soc., **Just Accepted Manuscript** • DOI: 10.1021/jacs.7b10688 • Publication Date (Web): 29 Nov 2017

How Solid-Electrolyte-Interphase Forms in Aqueous Electrolytes

Liumin Suo [a], Dahyun Oh [b, c], Yuxiao Lin [d], Zengqing Zhuo [e,f], Oleg Borodin [g], Tao Gao [h], Fei Wang [g, h], Akihiro Kushima [i], Ziqiang Wang [i], Ho-Cheol Kim [c], Yue Qi [d], Wanli Yang [e], Feng Pan [f], Ju Li *[, i], Kang Xu* [g], Chunsheng Wang *[,h]

[a] Key Laboratory for Renewable Energy, Beijing Key Laboratory for New Energy Materials and Devices, Beijing National Laboratory for Condensed Matter Physics, Institute of Physics, Beijing, 100190, China

[b] Biomedical, Chemical and Materials Engineering Department, San José State University, CA 95112, USA

[c] IBM Almaden Research Center, San Jose, CA 95120, USA

[d] Department of Chemical Engineering and Materials Science, Michigan State University, East Lansing, MI 48824, USA

[e] Advanced Light Source Lawrence Berkeley National Laboratory, Berkeley, CA 94720, USA

[f] School of Advanced Materials, Peking University, Peking University Shenzhen Graduate School, Shenzhen 518055, China

[g] Electrochemistry Branch, Sensor and Electron Devices Directorate, U. S. Army Research Laboratory, Adelphi, MD 20783, USA

[h] Department of Chemical and Biomolecular Engineering, University of Maryland, College Park, MD 20742, USA

[i] Department of Nuclear Science and Engineering, Department of Materials Science and Engineering, Massachusetts Institute of Technology, Cambridge, Massachusetts 02139

* Corresponding authors: liju@mit.edu; conrad.k.xu.civ@mail.mil; cswang@umd.edu

Abstract

Solid-electrolyte-interphase (SEI) is the key component that enables all advanced electrochemical devices, the best representative of which is Li-ion battery (LIB). It kinetically stabilizes electrolytes at potentials far beyond their thermodynamic stability limits, so that cell reactions could proceed reversibly. Its *ad hoc* chemistry and formation mechanism has been a topic under intensive investigation since the first commercialization of LIB 25 years ago. Traditionally SEI can only be formed in non-aqueous electrolytes. However, recent efforts successfully transplanted this concept into aqueous media, leading to significant expansion in the electrochemical stability window of aqueous electrolytes from 1.23 V to beyond 4.0 V. This not only made it possible to construct a series of high voltage/energy density aqueous LIBs with unprecedented safety, but also brought high flexibility and even "open configurations" that have been hitherto unavailable for any LIB chemistries.

While this new class of aqueous electrolytes has been successfully demonstrated to support diversified battery chemistries, the chemistry and formation mechanism of the key component, an aqueous SEI, has remained virtually unknown. In this work, combining various spectroscopic, electrochemical and computational techniques, we rigorously examined this new interphase, and comprehensively characterized its chemical composition, micro-structure and stability in battery environment. A dynamic picture obtained reveals how a dense and protective interphase forms on anode surface under competitive decompositions of salt anion, dissolved ambient gases and water molecule. By establishing basic laws governing the successful formation of an aqueous SEI, the in-depth understanding presented in this work will assist the efforts in tailor-designing better interphases that enable more energetic chemistries operating farther away from equilibria in aqueous media.

Introduction

Electrolytes in electrochemical devices provide an ionic pathway between anode and cathode. In advanced batteries, electrodes are often pushed to work at extreme potentials in order to maximize the energy output. These potentials situate far beyond the thermodynamic stability limits of electrolyte components (salt ions, solvent molecules), hence irreversible

decomposition reactions occur. In certain (but not all) scenarios, such decompositions produce dense solid products, which deposit on electrode surfaces, preventing sustained electrolyte decomposition while still allowing electrochemical reactions to proceed. Such an independent passivation phase is named solid-electrolyte-interphase (SEI) after its electrolyte nature, i.e., insulating to long-range electron transport but conductive to ions of significance to the cell reactions. Li-ion battery (LIB) chemistry owes its excellent reversibility to SEI existence on graphitic anodes, where Li^+-intercalation occurs at ~0.10 V vs. Li, far below the reduction potentials of most electrolyte solvents.[1,2] Emerging battery chemistries beyond Li-ion are expected to heavily rely on the ability to tailor-design and manipulate SEIs on new electrode materials.[3]

Thanks to the commercial success of Li-ion batteries, intensive investigations have been conducted in the past two decades on SEI formed in carbonate-based non-aqueous electrolytes. Significant knowledge has been achieved regarding the chemistry,[4] morphology[5] and formation mechanism[4,6] of these carbonate-originated SEIs, while various approaches have become available to tailor their properties based on the understanding of their chemical composition and morphology.[7] However, mysteries still exist, and debate arise often, because of the nano-scale presence and the *ad hoc* formation nature of SEI, and the sensitivity to ambient contaminates.

On the other hand, SEI has always been associated only with non-aqueous electrolytes, because none of the decomposition products from water, i.e., H_2 and hydroxide at anode or O_2 and H^+ at cathode, could deposit in solid state on electrode surfaces and form a protective interphase. This general consensus was overturned by the recent groundbreaking work of Suo et al, who successfully managed to form the very first aqueous SEI by altering Li^+-solvation sheath structure with super-concentration.[8] The expanded electrochemical stability window of the so-called "water-in-salt" electrolyte (WiSE), along with its later variations, enabled a series of high voltage/high energy density aqueous battery chemistries that deliver energy densities and cycling stability approaching the state-of-the-art LIB based on non-aqueous electrolytes, but without the safety concern of the latter,[9-13] Furthermore, the ambient-insensitivity of the aqueous nature also brought unprecedented flexibility to the form-factor of LIBs, making a cell of "open configuration" possible for the first time.[14]

In this work, combining various in-situ/operando techniques and molecular dynamics (MD) simulations, we rigorously examine this new interphase that could induce transformational advance in battery materials and technology. The in-depth investigation establishes a few key guiding principles to improve the chemical durability of aqueous SEIs for future high voltage aqueous electrochemical devices.

Results and Discussion

(1) Live-formation of aqueous SEI

At pH=7, the cathodic stability limit of water locates at 2.626 V, below which water molecule starts to decompose reductively, evolving H_2 and OH^-. Theoretically this reaction sets the lowest limit for an anode material to operate in dilute aqueous electrolytes. In aqueous electrochemistry, a common practice to manipulate this lowest cathodic limit is to suppress the activity of proton by adjusting the pH-value of aqueous solutions.[14] However, even in the strongly alkaline electrolyte (pH=14), hydrogen evolution still occurs at 2.213 V vs. Li, which is too high to accommodate most of the anode materials desired by battery scientists. Besides, a downshift of O_2 evolution potential would occur simultaneously with increasing pH, keeping the gap between the anodic and cathodic limits constant at 1.23 V. This gap, known as the electrochemical stability window of aqueous electrolytes under thermodynamic equilibria, is defined by Pourbaix diagram. The slightly higher voltage of 1.5 V realized in existing aqueous battery chemistries [15,16] was the result of "kinetic overpotentials" of H_2 or O_2 evolutions, which depends on salt concentration, catalytic activity of the electrodes and applied currents. This slight kinetic expansion is only effective when the devices are tested at high rates, otherwise parasitic reactions (H_2 evolution at anode in particular) would become pronounced enough to compete with the cell reactions, significantly decimating the coulombic efficiencies of the latter. Hence, a voltage window expansion would only be meaningful for the battery applications with the formation of an interphasial barrier, similar to SEI in LIB.

In order for such an aqueous SEI to form, its precursor must meet one primary prerequisite, i.e., its reductive decomposition has to occur at a potential before major water

decomposition occurs, so that interference from the competitive H_2 evolution could be minimized. In the seminal work of Suo et al.[8], this was achieved by super-concentration (21 m) of LiTFSI, where the altered Li^+-solvation sheath structure promotes the reduction of anion TFSI from 1.40 V to a higher range (2.30~2.90 V depending on the reaction pathways), thus making it possible to form a dense and protective interphase based on LiF. Since this range significantly overlaps with the H_2 evolution potential (~2.60 V, at pH=6.8 for LiTFSI/H_2O), at least part of the irreversible capacity observed during the first charging should be contributed by the water decomposition, along with the reduction of TFSI. Figures 1a, 1b, 1c and 1d showed voltage profiles of the aqueous Li-ion full cells based on $LiMn_2O_4$ cathode and Chevrel-phase Mo_6S_8 anode in aqueous electrolytes at four different LiTFSI concentrations (1 m, 5 m, 10 m and 21 m). Both these electrodes are intercalation-type materials known for their excellent rate capabilities. The irreversible capacities, defined as the difference between the charge and discharge capacities in the first full cycle, showed strong dependence on salt concentration. Since both Mo_6S_8 anode and $LiMn_2O_4$ cathode have two characteristic Li^+-intercalation plateaus (~2.2 V/~2.5 V and ~4.1 V/~4.3 V vs. Li, respectively, depending on salt concentrations), ideally the full cell voltage should consist of two corresponding plateaus at ~1.5 V and ~2.1 V. As described previously, however, the higher plateau (which corresponds to full lithiation of Mo_6S_8 anode at 2.20 V vs. Li) cannot be accessed by diluted aqueous electrolytes due to extensive water decomposition, as indicated by the long flat H_2O decomposition plateau above 1.80 V (Figure 1a). As salt concentration increases, this upper flat plateau gradually shifted up (Figure 1b and 1c), accompanied with rapid decrease in the irreversible capacity (Figure S1). Meanwhile, the second Li^+-intercalation plateau at ~2.0 V appears, until at 21 m (Figure 1d), where the columbic efficiency reached 86 %, with only ~7.7 mAh/g out of 43 mAh/g overall capacity is irreversible. This irreversible part is believed to be mostly attributed to the SEI formation due to the reduction of TFSI and dissolving gases (CO_2 and O_2) reductions.

To quantitatively study this formation chemistry, an *in-situ* electrochemical analysis technique, i.e., differential electrochemical mass spectrometry (DEMS), [17] was used to monitor the gaseous compounds during the initial charging process and how they change with the salt concentration. Figure 1e, 1f, 1g and 1h display the DEMS collected from the identical

aqueous full Li-ion cells. As expected, in diluted solution (1 m), the water splitting overwhelmed the irreversible process, cumulatively producing 84117 nmol H_2 and 22438 nmol O_2 continuously when the cell is charged above 1.8 V (Figure 1e). It should be noted here that the amounts of H_2 and O_2 do not precisely obey the 2:1 stoichiometric ratio, revealing that the irreversible process, even in the diluted electrolyte, is not entirely corresponding to water splitting, while other competing processes such as Li^+-intercalation and anion reduction also exist simultaneously. With increasing LiTFSI concentration, the water decomposition at cathode surface is apparently suppressed by much higher extent than at anode surface, as O_2 almost completely disappears at 10 m, while H_2 continues to generate until 21 m (Figure 1g and 1h). This distinction is consistent with the general knowledge that the kinetics of H_2 evolution is much facile than O_2 evolution, and serves as a strong rationale for the so-called "cathodic challenge", [13,18] i.e., that the most severe challenge for high voltage aqueous batteries comes from the stabilization of anode rather than cathode surface. At 21 m (the "water-in-salt" electrolyte, or WiSE), the O_2 evolution is completely eliminated during the 1st charging process, while negligible amount (43 nmol) of H_2 is still detected (Figure 1h), corresponding to ~0.00115 mAh/g irreversible capacity. In other words, in the overall irreversible capacity obtained in WiSE during the 1st cycle (~5 mAh/g), only ~0.02% is contributed by the water reduction, while, reductions of other species including TFSI account for the majority of the irreversible process. Although this percentage distribution could be over-estimated in favor of TFSI due to the delayed diffusion of H_2 across electrolyte and to mass spectrometer, qualitatively it still shows how much super-concentration has promoted TFSI-reduction in its competition with water decomposition. It was this preferential reduction of salt anion that is responsible for the opportunity of forming an SEI in an aqueous media. Examining the voltage profile and capacity for the 2nd cycle (Figure 1d), one could visually conclude that this irreversible process essentially disappears. However, as the coulombic efficiency indicates, trace amount of water decomposition persists (Figure 1h), until SEI is perfected in at least a few more cycles following the very 1st charging process [8].

The chemical composition and distribution of SEI throughout the 3D-porous electrode is further investigated using time-of-flight secondary ion mass spectrometry (TOF-SIMS) in both negative and positive modes (Figure 2, Figure S2~S4). Ga-ion sputtering generate five

negative species (Figure S3), including F^- (m/e=19), S^- (m/e=32), O^{2-} (m/e=16), and OH^- (m/e=17), with F^- being the dominant. This is consistent with our earlier conclusion that LiF exist as the main SEI component on the cycled anode surface, as revealed by X-ray photoelectron spectroscopy (XPS) and Energy-dispersive X-ray spectroscopy (EDX)[8]. The presence of O-containing species, previously not revealed by XPS, implies that ingredients other than LiF also exist in this aqueous SEI.

In order to eliminate the possible interferences from poly(tetrafluoroethylene) (PTFE) binder and carbon black conductive additive in the composite anode, the positive mode of TOF-SIMS was also measured under the same condition, which detects positive cluster species $(Li_2F)^+$ (m/e=33) beside naked Li^+ (Figure S4). Assuming that F^- in negative mode comes from PTFE, then C^+ (m/e=12) and related C-F fragments (CF^+ m/e=31, CF_2^+ m/e=50, CF_3^+ m/e=69) should also be detected in positive mode.[19,20] In fact, their absence confirms that the dominant F^- comes from LiF in the SEI. The depth-profiles of SEI was established by etching a selected area on the electrode surface, which was subject to continuous Ga-ion sputtering (Figure 2). The LiF-based interphasial species was revealed to penetrate the anode surface (Figure 2a), whose intensity reaches a maximum at 600~800 nm followed by gradual decay. It should be cautioned here that this maximum depth should not be mistaken as SEI thickness, considering that the electrode surface is highly porous; rather, it reflects the distribution of SEI species throughout the micro-structure of the porous electrode.

In view of the possibilities of minor interphasial species other than LiF, two additional surface-sensitive techniques, XPS (Figure 3a ~ 3f) and soft-X ray absorption spectra (sXAS) (Figure 3g ~ 3i), were also used to provide a more comprehensive chemical picture. The former, aimed to describe qualitatively the SEI components and its space distribution, was conducted with Ar^+-sputtering at different intervals, while the latter, with the purpose to relate SEI chemical composition to relative potential, was carried out on Mo_6S_8 at different states-of-charge (SOC) of 1.4 V, 1.6 V, 1.9 V, 2.0 V and 2.3 V, respectively. In both experiments, Mo_6S_8 electrodes were recovered from cycled cells at designated potentials. Both XPS and SXAS revealed the presence of Li_2CO_3 and Li_2O on the surface of cycled electrode (Figure 3), which revised our previous understanding of the aqueous SEI formed in WiSE[8]. C 1s and O 1s spectra in Figure 3a detected strong signal between 289~290 eV and

531.5 eV (Li_2CO_3 or alkylcarbonate) on the cycled Mo_6S_8 electrode; however, with Ar^+-sputtering the abundance of Li_2CO_3 decreases steadily (Figure 3b). Li_2O, on the contrary, increases (Figure 3 c and 3d), suggesting an SEI of layered-structure, with Li_2O in the inner and Li_2CO_3 in the outer layers, respectively. C and O K-edge SXAS spectra not only confirmed the existence of both Li_2CO_3 and Li_2O in SEI, but also further verify that their formation occurs above 1.6 V of $LiMn_2O_4/Mo_6S_8$ cell (Figure 3g 3h and 3i). With increasing charge voltage, the intensity of Li_2CO_3 and Li_2O signal gradually became stronger, no matter in deep (100 ~ 200 nm) or shallow (< 10 nm) local regions. The only exception is the fully charged electrode (2.3 V, SOC 100 %), whose intensity is significantly lower due to the damage from water decomposition, because SEI has not been completely formed in this first cycle. Thus, it again indicated that SEI formation process has to compete with H_2 evolution, and its protection of the electrode against water decomposition would need certain number of cycles to take full effect. After 16 cycles, Li_2CO_3 could be clearly detected at 100% SOC (2.3 V, Figure. S5).

Both XPS and sXAS confirmed the presence of F (Figure 3e and S6~S7), which came from two different sources: TFSI from the residual lithium salt or its partially fragmented form, as evidenced by F 1s at ~689 eV (C-F species), and simple fluoride as evidenced by F 1s at 685~686 eV (F^-). The latter will only be revealed after etched by Ar^+- or Ga^{3+}, respectively. Apparently, TFSI reduction occurs at locations near the anode surface, leading to an SEI structure with the more completely reduced species reside in the inner region, such as simple inorganic salts LiF and Li_2O. This layered-structure is quite similar to SEIs formed in non-aqueous electrolytes.[21,22] With F and O apparently coming from the reduction of TFSI and water, the presence of Li_2CO_3 may appear puzzling as there seems to be neither source of C (such as organic carbonate ester in non-aqueous electrolytes) nor mechanism to form O-C=O species (electrochemical oxidation of carbonaceous materials from composite electrodes is essentially impossible due to the prohibitively high energy barriers). We attributed its formation to the dissolved CO_2 from the ambient, as all electrolyte preparation and cell assembly were conducted in ambient atmosphere. The slight acidic nature of WiSE (pH=6.5~6.8) [8] confirms this hypothesis, as LiTFSI should render the aqueous solution slightly basic (pH>7) when prepared under degassed conditions.

(2) Formation mechanism of aqueous SEI

The chemical composition of SEI implies that two possible pathways contribute to its formation process: (1) reduction of anion complexes or clusters; and (2) reduction of O_2 and CO_2 dissolved in the electrolyte (Figure 4d). The former provides the source for LiF and the latter for both Li_2CO_3 and Li_2O. Both reactions are under heavy influence of the salt concentration. Raman spectra reveals intensified cation-anion interactions as salt concentration increases (Figure 4a), in which S-N-S bending peak shifts evidently from 744 cm^{-1} (1 m) to higher wavenumber at 748 cm^{-1} (21 m), because of the drastic change in cation (Li^+) and anion ($TFSI^-$) solvation structures and the corresponding electron density distributions on the TFSI. According to Li-TFSI distance [23], the cation-anion clusters could be classified into free anion (FA)-(#Li^+=0)-740 cm^{-1}, loose ion pair (LIP)-(#Li^+=1)-744 cm^{-1}, intimate ion pair (IIP)-(#Li^+=1)-747 cm^{-1} and aggregate ion pair (AGP)-(#Li^+=2)-748 cm^{-1}, respectively, according to fitted Raman spectra (Figure 4a~ 4c). The specific proportion of these four cation-anion coordination structures is listed in Table 1, which is found in good agreement with the analysis of Fourier-transformed infrared (FTIR) measurements and MD simulations for 10m and 21m.[24] In WiSE (21m), the percentage of AGP is ~82%. As our previous MD simulation showed,[8,24] there is no sufficient water molecules at this high salt concentration to fully solvate all Li^+ and separate them from TFSI. Instead, Li^+ is coordinated by slightly less than two oxygens from TFSI, and slightly more than two oxygens from water. In such extended aggregates, $TFSI^-$ is often shared by two or three Li^+.[24] Multiple Li^+ coordination by the $TFSI^-$ anions stabilized the transferred electron during reduction resulting in higher reduction potential. Earlier quantum chemistry study of the reduction reaction has identified $Li_2(TFSI)^+$ (Figure 3b) as the representative of highly aggregated ion aggregates in WiSE that would be reduced at the highest potential of 2.9 V, which might provide the essential basis for a SEI formation mechanism that could compete with water reduction.

On the other hand, in Li^+-conducting electrolytes, the theoretical reduction potentials of most dissolved gases (O_2 and CO_2) usually situate at higher values:

$4Li^+ + O_2 + 4e^- \rightarrow 2Li_2O$; $E° = 2.91$ V;

$2Li^+ + 1/2O_2 + CO_2 + 2e^- \rightarrow Li_2CO_3$; $E° = 3.82$ V

In diluted aqueous electrolytes, these gaseous solute never gets the opportunity of forming solid deposits on electrode surfaces as their reduction products would quickly hydrolyze and dissolve:

$Li_2O + H_2O \rightarrow 2Li^+(aq) + 2OH^-(aq)$

$Li_2CO_3 + H_2O \rightarrow HCO_3^-(aq) + 2Li^+(aq) + OH^-(aq)$

Thus, the scenario of an SEI consisting of Li_2CO_3 and Li_2O would be beyond possibilities in diluted aqueous solutions. It was the super-concentration of LiTFSI in WiSE that makes it possible for LiF, Li_2CO_3 and Li_2O to deposit on anode surface without dissolution. Simultaneously, the super-concentration also results in a significant depletion of free water fraction in WiSE (15% at 21 m LiTFSI). Hence, much fewer water molecules are available to be adsorbed on the electrode surface, which is often the first step of water decomposition reactions. Moreover, in the highly concentrated LiTFSI-based electrolytes the CF_3-groups of $TFSI^-$ anions tend to preferentially adsorb at the negative electrode surfaces potentials above 2.5 V vs. Li/Li^+. This preferential adsorption further facilitates LiF formation.[25] The fortuitous combination of all these factors leads to the formation of a composite SEI that consists of LiF, Li_2CO_3 and Li_2O, with LiF being the dominant ingredient.

(3) Solubility and continuous growth of aqueous SEI

To support reversible cell reactions, SEI must remain stable in the bulk electrolyte against both electrochemical reactions and chemical dissolution. Given that water is one of the most powerful solvents, as characterized by its high dielectric constant, dipole moment and acceptance/donor numbers, an aqueous SEI faces much more severe challenges than its non-aqueous counterpart does. LiF-rich SEI cannot form on Mo_6S_8 anode in 1 m LiTFSI electrolyte, as the Mo_6S_8 anode mainly induces water reduction reaction rather than lithiation, as demonstrated by the low discharge capacity and low coulombic efficiency in Figure 5a.

This is because the sustained hydrogen evolution occurs at higher or similar potential as the TFSI reduction, preventing LiF deposition in dense form and the subsequent constitution of a passivation layer. In addition, the SEI components also suffer higher solubility in a dilute aqueous solution, which further increases the difficulty in building up a robust SEI. For example, even the least soluble lithium salt, LiF, remains slightly soluble in neat water (about 0.04 mol/L),[26] which is high enough to disrupt an SEI based on LiF in the dilute electrolytes considering the nanometric existence of interphase. This constitutes the main reason why a $LiMn_2O_4/Mo_6S_8$ full cell cannot charge/discharge in 1 m LiTFSI, even after an effective SEI was pre-formed on Mo_6S_8 anode in WiSE. In this scenario, the pre-formed SEI consisting of LiF, Li_2CO_3 and Li_2O obviously falls apart by dissolving in the dilute electrolyte (Figure 5b). Thus, super-concentration is not only required for the formation process of SEI, but also necessary to maintain and repair such an aqueous SEI. On the other hand, the excellent cycling stability of various battery chemistries demonstrated in WiSE implies that the aqueous SEI formed in WiSE must be highly resistant to the dissolution by the water molecules therein.[8-13] Here the "Common Ion Effect" exerts by the extremely high Li^+-population in WiSE is a critical pre-requisite for keeping these inorganic lithium salts in solid form and maintain the composite SEI.

Even in the best non-aqueous electrolyte, the continuous growth of formed SEI is inevitable, as indicated by the parasitic processes revealed by the high precision Coulometric studies.[27,28] The instability of SEI can also be reflected in the long-term storage and self-discharge experiments. As Dahn and coworkers taught, an electrolyte or the durability of an SEI would experience the most rigorous test when it is exposed to extreme potentials.[25] To understand how robust the aqueous SEI is, the decay of open circuit voltages (OCV) were monitored for a series of fully charged aqueous Li-ion cells. As Figure 6 shows, the OCV significantly stabilizes if the SEI was formed either at a low rate of 0.1 C (Figure 6 a), or after extended cycling at 1 C (Figure 6 b). These results basically manifest that the integrity of SEI is only dependent on the duration of time that the electrolyte spent at the forming potentials. The best quality of SEI was obtained within 10 cycles at 1 C, as demonstrate by the stable potential without any evident drop for 150 hours. C and O K-edge sXAS spectra of cycled Mo_6S_8 lead to the same conclusion, where the intensities for both Li_2CO_3 and Li_2O reach high

level only after multiple (16) cycles (Figure 6c) or at low (0.2 C) charging rate (Figure S5).

In actual battery environments, the formation process of SEI is rather complicated, which is difficult to be described by a simple equation. Here we adopted the model of diffusion-limitation for the growth of non-aqueous SEIs: [27,29]

$$\frac{dx}{dt} = \sqrt{\frac{\kappa}{2}}\ t^{-\frac{1}{2}} \qquad (2)$$

Where κ is a constant dependent on electrolyte/electrode and temperature, t is time, x is the hypothetic thickness of an idealized SEI, and dx/dt is SEI growing rate.

A few assumptions were made here: (1) SEI component is homogeneous and unchanged with SEI layer thickness (x), (2) SEI is uniform without any defects like cracks or holes. Based on above oversimplifications (most of which are almost certainly not true but nevertheless provide a good-enough approximation), we measured electrochemical impedance spectra at different cycles (Figure 6d). Nyquist and Bode plots at OCV stage showed only one semi-circle in medium frequency (~2400 Hz) corresponding to charge-transfer resistance (R_{ct}), while no response from SEI component occurs in resting process. Once the cell has been cycled 10 cycles, a new semi-circle appears in high frequency range (~10^5 Hz), which was assigned to SEI.[5,30] This semi-circle becomes more obvious after 20 cycles, indicating its full formation. The fitted results using an equivalent circuit (Figure 6d inset) show that the resistance of SEI (R_{SEI}) also increases with the cycling, with Coulombic efficiency gradually approaching 100%. In order to exclude any interference from the cathode side, the EIS of the anode was also collected in three-electrode device after the initial 2 formation cycles (Figure S6).

Among the many models and theories to predict SEI thickness, electron tunneling model (ETM) proposed by Peled is widely accepted, which states that SEI thickness is determined by the electron tunneling range[31]. DFT calculations were employed to predict the electronic tunneling barriers and SEI thickness.[32] Figure 6e shows the energy levels of anode materials (such as Li, Mo_6S_8 and Li_4MoS_8), SEI component (such as LiF), and electrolyte, as highlighted in yellow, green and grey, respectively. The DFT computed relative position of the Fermi level (ε_f), band gaps (E_g), and work function (Φ) of each material, together with the density of states (DOS) around the band gap of LiF, are aligned with respect to a common

reference, the vacuum, which is set as 0 eV for a better comparison. Therefore, if any excess electron from the electronic conducting electrode tunnels through the electronic insulating SEI component to reach electrolyte, it has to overcome the electronic tunneling energy barrier (ΔE_t) from the Fermi level (ε_f) of anode material to the bottom of the conduction band of SEI component. According to Figure 6f, the electronic tunneling energy barrier can be calculated, as shown in Equation 3 and the electronic tunneling probability is assumed as shown in Equation 4 to a very small value of e^{-40} :

$$\Delta E_t = E_g(SEI) - \Phi(SEI) + \Phi(anode) - E_g(anode) \quad (3)$$

$$T = \frac{16\varepsilon_f \cdot \Delta E_t}{(\varepsilon_{f+}\Delta E_t)2} e^{-\frac{4\pi d}{h}\sqrt{2m \cdot \Delta E_t}} \quad (4)$$

the critical thickness of SEI, d^*, that blocks electron tunneling can thus be estimated. Actually, if we assume that SEI layer component is only composed by a single crystal insulating LiF while ignoring any defect and grain boundary, its thickness under this ideal condition can be determined (Figure 6g). The computed electron tunneling barrier and the thickness of SEI layer for both unlithiated Mo_6S_8 and full lithiated $Li_4Mo_6S_8$ are summarized in Table S1. The former behaves as a metallic conductor, on which the critical SEI thickness is ~1.6 nm for LiF. However, the latter $Li_4Mo_6S_8$ became an insulator with band gap of 1.46 eV, which will significantly decrease the electronic tunneling barrier and increase the critical SEI thickness to ~ 2.4 nm. Experimentally, we have observed using high solution TEM that SEI thickness ranges between 10 nm and 15 nm, similar to non-aqueous SEIs observed previously (Figure 6g). We believe that the above difference can probably be ascribed to the following factors. (1) SEI in real life is composed not only by LiF but also Li_2O and Li_2CO_3 (Figure 2 and 3), among which pure LiF has the largest tunneling barrier, thus the mixture of which is expected to have increased SEI critical thickness[32]; (2) The significant mismatch in the lattice parameter between Mo_6S_8 and LiF inevitably induces tension in SEI, which further intensifies with the volume expansion of Mo_6S_8 after lithiuation. This will also decrease the band gap of LiF and increase the critical thickness of SEI[32]; (3) Inhomogeneous SEI formation process including grain boundary, cationic and anionic defects and multi-components, which makes SEI far from being perfectly dense; and (4) other potential electron transport mechanisms may also be involved, resulting from the formation of defects and polarons. These effects

make it possible for an electron to tunnel not just once ("ballistic"), but multiple times, giving rise to more diffusive hopping transport behavior. As the SEI grows thicker, it might be necessary for species like $Li_2(TFSI)^+$to partly penetrate the SEI through diffusion, before meeting the electron and get reduced. These diffusive mechanisms underline the parabolic kinetic law (2), when *x* has grown thick enough. When *x* is ultra-thin and single-tunneling is sufficient, the Cabrera-Mott regime growth law is more appropriate.

Based on above results, we now can envision a comprehensive picture of how an aqueous SEI forms in aqueous electrolytes. In the super-concentrated (21 m) solution of LiTFSI in water, extensive ionic cluster forms due to the limited availability of water molecules. The intimate interaction between cation and anion leads to two consequences: (1) the activity of water molecule is so suppressed that the electrolyte becomes rather resistant against oxidation at cathode surface, and (2) the reduction potential of TFSI in the ionic clusters is significantly raised to levels competitive with H_2 evolution.

During the SEI formation, there are actually three sources contributing to the irreversible reduction reactions: (1) dissolved O_2 and CO_2; (2) salt anion and (3) water molecule. Among them, water decomposition is purely parasitic because it does not contribute to SEI component while depleting lithium source. The competition among these irreversible reactions would determine whether an SEI can be formed or how stable it is against dissolution by aqueous electrolytes. The formation of aqueous SEI might experience a few distinct stages:

(1) The reductions of dissolved gas and TFSI (between 1.9 ~ 2.90 V), where the electrode potential still sits comfortably within the electrochemical stability window of the electrolyte. The reduction products are expected to adhere to the electrode surface, but the formation of complete SEI needs long time (i.e. few cycles in galvanostatic charge/discharge cycles). When the electrode sits at a low potential long enough, the final reduction products (LiF, Li_2O and Li_2CO_3 start to form. The insolubility of these simple inorganic salts in WiSE provides better adhesion to anode surface, thus effectively shielding the anode surface and prevented further H_2-evolution. It is during this stage that robust and protective SEI come into shape, although it will take more than one cycle to consolidate its chemical and mechanical durability.

(2) The co-existence of all irreversible reactions (< 1.9 V), where the reduction of water starts with H_2-evolution. H_2 gas bubbling, even at nanoscale, would pose significant erosion risk. This reaction competes with the reduction of dissolved gas and TFSI, and interferes the adhesion of their products to the anode surface;

(3) It should be kept in mind that, even during the long-term cycling and storage after SEI is formed, SEI still faces the sustained dissolution, corrosion, cracking and reforming, and the presence of super-concentrated electrolyte is essential to repair and maintain such an aqueous SEI.

Conclusion

In this work we rigorously characterized the chemistry, micro-structure, formation mechanism and stability/durability of a new SEI formed in aqueous electrolyte. Using a combination of *in-situ/ex-situ* spectra techniques, we analyzed its exact chemical compositions, and demonstrated how reductive decompositions of TFSI, dissolved O_2 and CO_2, and water molecule compete in the very first formation process. Several key factors responsible for the successful formation of aqueous SEI were identified, which include the salt concentration, chemical structure of salt anion, possible reduction products and their solubilities in aqueous electrolyte, and the formation condition. A model for the durability and aging of aqueous SEI was also proposed. This molecular-level understanding about this new interphasial chemistry establishes a guiding principle to tailor-design of better aqueous SEI that helps to eventually resolve the "cathodic challenge" in high-voltage aqueous batteries.

Figures and Captions

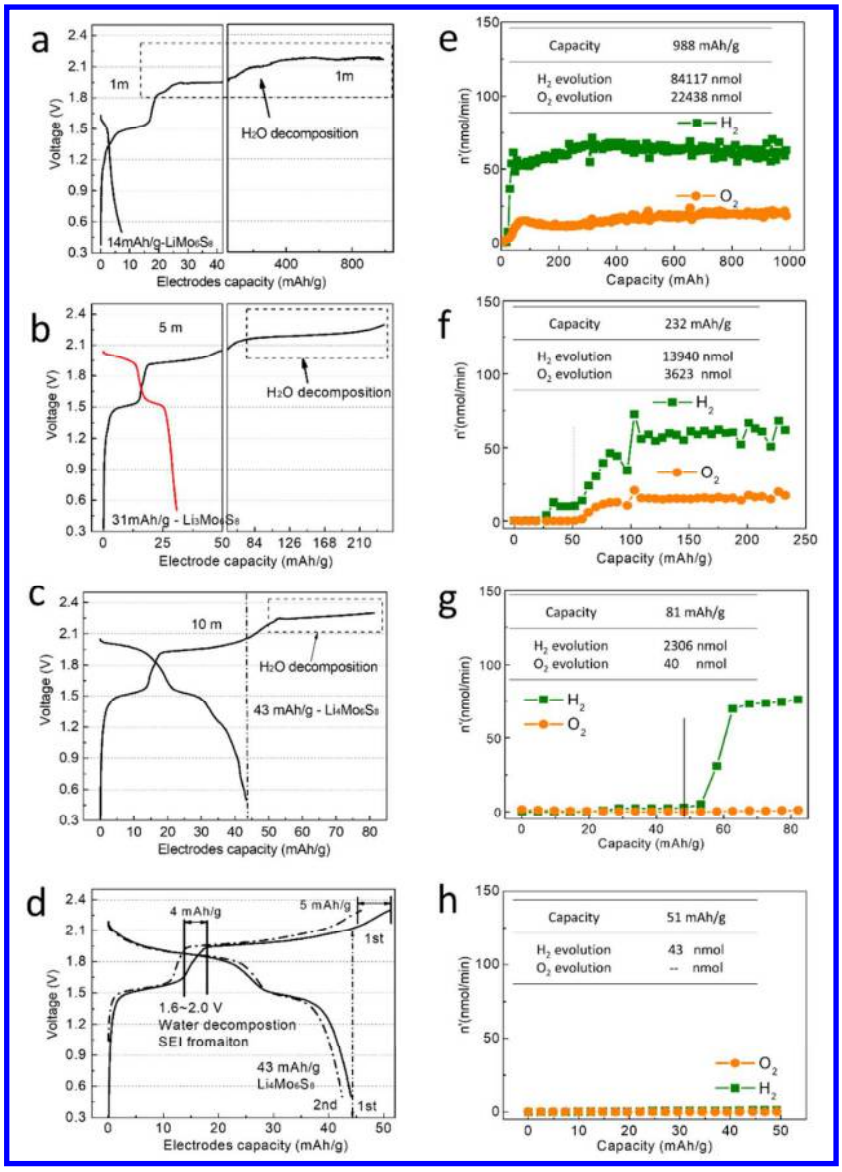

Figure 1. **(a) ~ (d):** Voltage profiles for the first charge-discharge profiles of full Li-ion cells constructed with Mo_6S_8 anode and $LiMn_2O_4$ cathode and cycled in four aqueous electrolytes of different salt concentrations. In these full cell configurations the anode and cathode are coupled at $LiMn_2O_4/Mo_6S_8$ = 2:1 by weight. **(e) ~ (h):** H_2 and O_2 evolution monitored during the first charging process using differential electrochemical mass spectrometry (DEMS) in these same aqueous full Li-ion cells

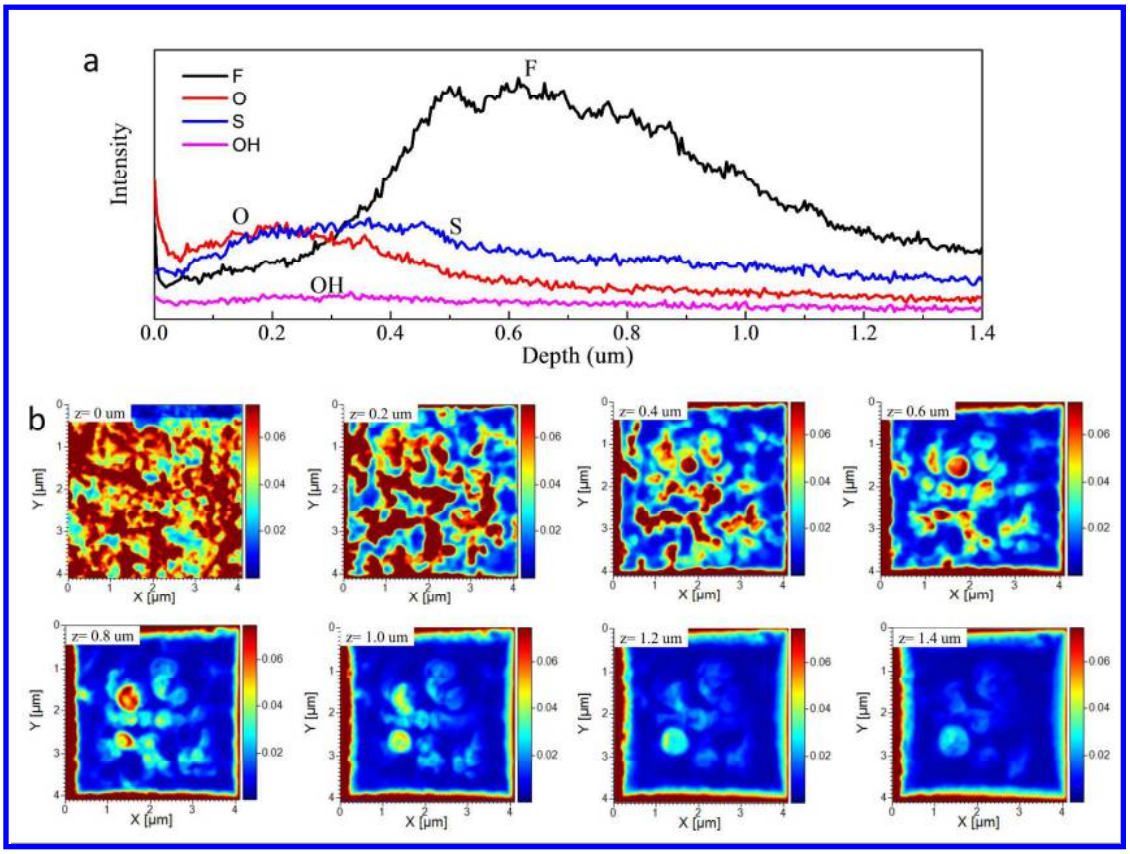

Figure 2. Time-of-Flight Secondary Ion Mass Spectrometry (TOF-SIMS) Analysis of cycled Mo_6S_8 electrode after being cycled for 40 times at 0.5 C (Negative mode). (a) TOF-SIMS depth-profiles of various chemical species, and (b) the variation of SIMS total intensity with the etching depth.

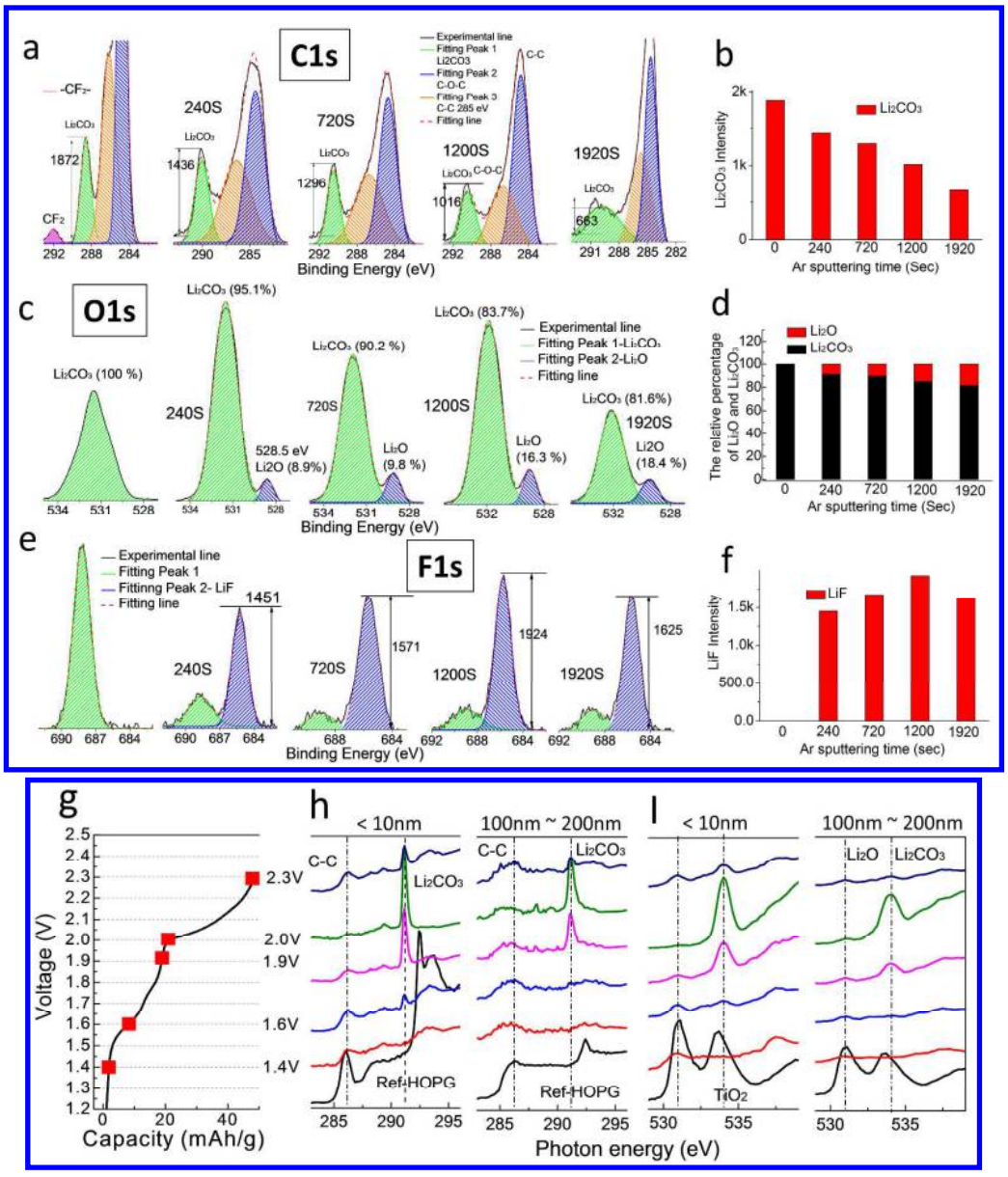

Figure 3 X-ray Photoelectron Spectroscopy (XPS) conducted on fully charged Mo_6S_8 with various Ar^+-sputtering intervals and Soft X-ray Absorption Spectroscopy (SXAS) on cycled Mo_6S_8 at different state-of-charge (SOC) in both bulk-sensitive TFY and surface sensitive mode corresponding to two detected penetration depths of < 10 nm and 100 ~ 200 nm respectively. (a) C1s spectra; (b) the intensity change of Li_2CO_3 with various etching durations from (a), (c) O1s spectra; (d) the relative intensity of Li_2O and Li_2CO_3 with the various etching durations of (c); (e) F 1s spectra; (f) the relative intensity of C-F and LiF with the various etching durations of (e); (g) the charge profile of full cell ($LiMn_2O_4$/ Mo_6S_8), (h) C K-edge sXAS spectra at different SOC (1.4 V, 1.6 V, 1.9 V, 2.0 V and 2.3 V) with highly oriented pyrolytic graphite (HOPG) as the reference, (i) O K-edge sXAS spectra at different SOC (1.4 V, 1.6 V, 1.9 V, 2.0 V and 2.3 V) with TiO_2 as the reference.

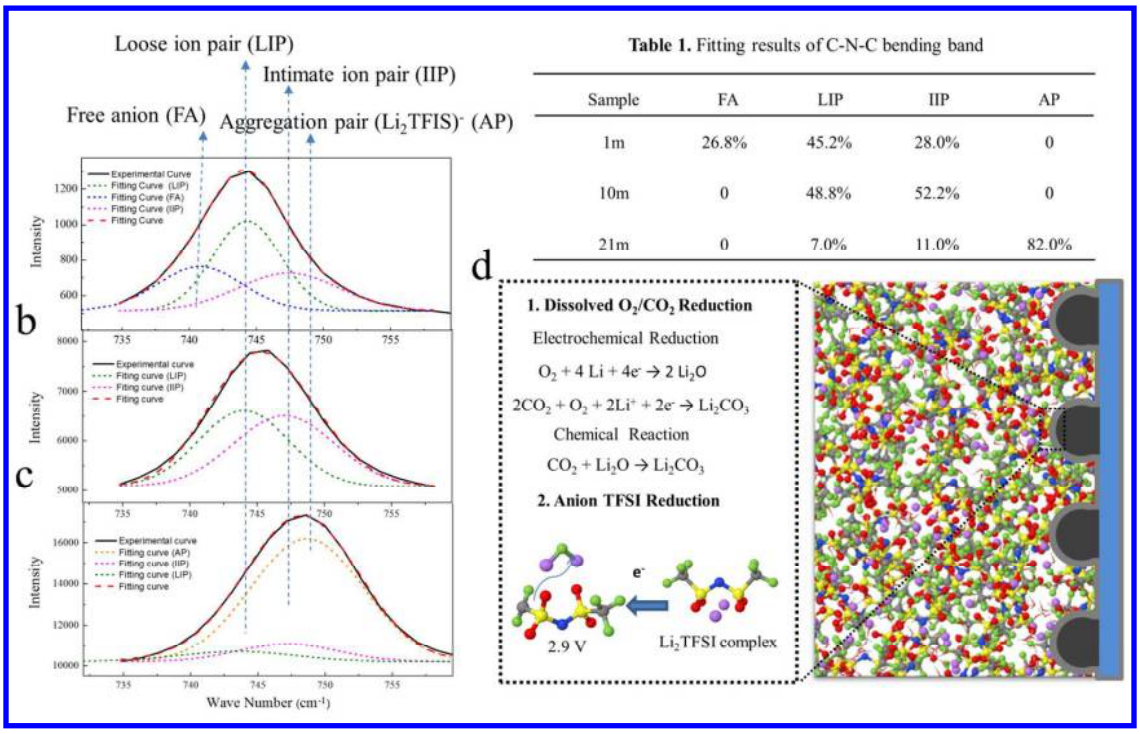

Table 1. Fitting results of C-N-C bending band

Sample	FA	LIP	IIP	AP
1m	26.8%	45.2%	28.0%	0
10m	0	48.8%	52.2%	0
21m	0	7.0%	11.0%	82.0%

Figure 4. Raman spectra of LiTFSI-H_2O electrolytes (a. 1m, b. 10m, c. 21m) and its corresponding cation-anion coordination structure (Table 1) (Free anion (FA), Loose ion pair (LIP), Intimate ion pair (IIP) and Aggregation pair (AIG)). (d) SEI formation mechanisms in Water-in-Salt electrolyte.

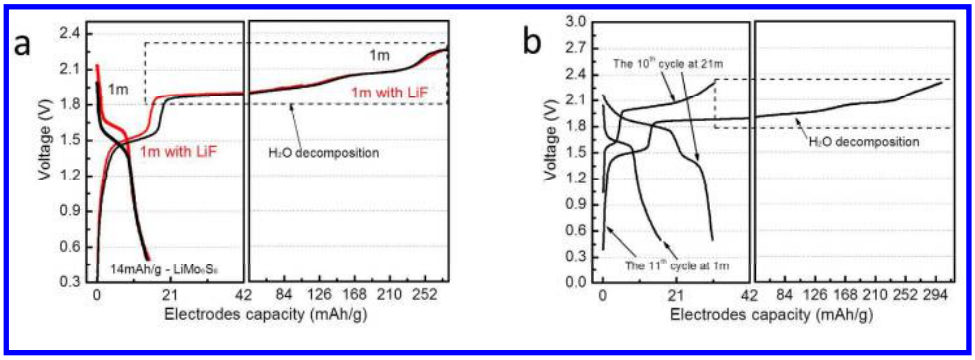

Fig. 5. The solubility of aqueous SEI and the related electrochemical performance of aqueous Li-ion $LiMn_2O_4/Mo_6S_8$ full cell. (a) in 1 m LiTFSI/H_2O with or without being saturated with LiF; (b) The same cell in 1 m LiTFSI/H_2O after an SEI was pre-formed in WiSE (21 m) for 10 cycles.

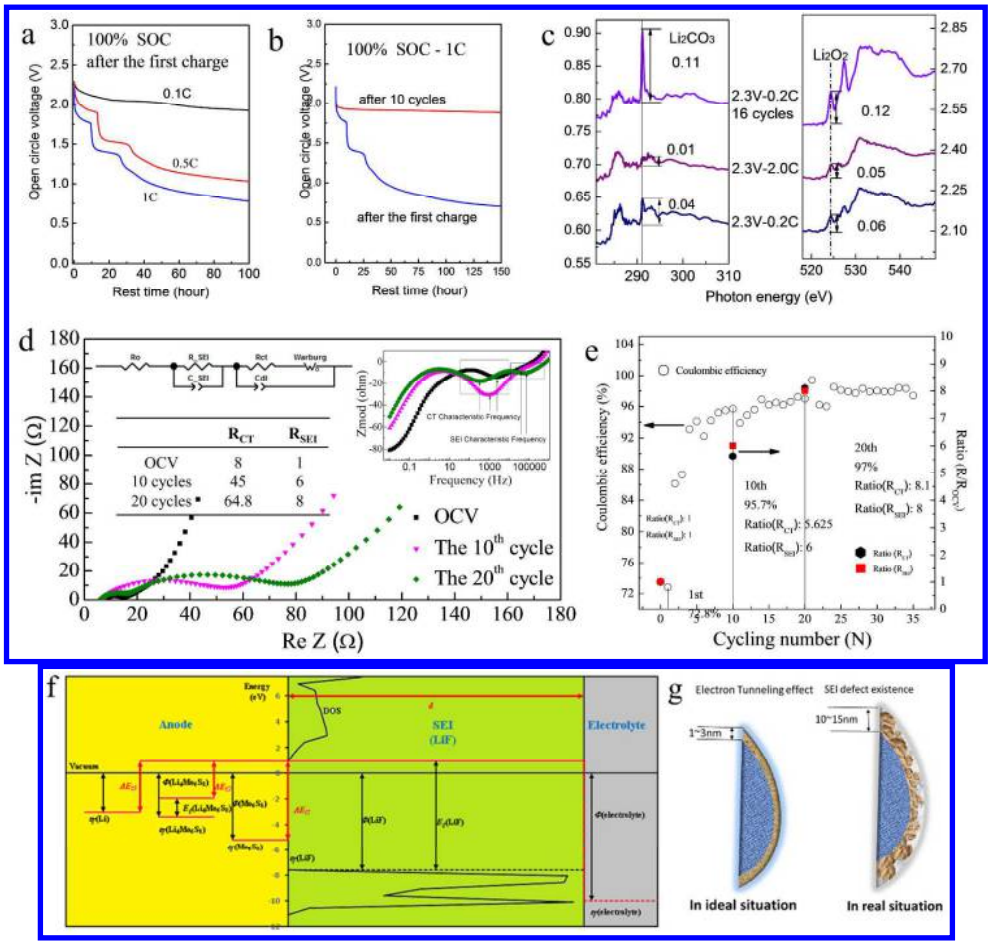

Figure 6. **The stability of aqueous SEI. (a)** and **(b)** Open circuit potentials (OCV) decays with rest time. **(a)** the cell is firstly fully charged to 2.3 V at different rate (C/5, C/2 and C), then rest at 100% SOC; **(b)** the cells are rested at 100% SOC after different cycles at high rate (1C); **(c)** C and O K-edge SXAS spectra of the aqueous SEI formed on Mo_6S_8 at different cycles (1 and 16 cycles) and rates (0.2 C and 2 C) in the surface-sensitive TEY mode with the detected penetration depth of < 10 nm; **(d)** ~ **(e)** Electrochemical Impedance Spectrum (EIS) at different cycles (full-cell after 24 h resting, 10 cycles and 20 cycles). **(d)** Nyquist plots with the insert of Bode plots and equivalent circuit fitting based on ESI experimental data; **(e)** the corresponding Coulombic efficiency; **(f)** Scheme of the ideal and actual SEI formations. (ii): ideal SEI formation dependent on electron tunneling effect, (ii) actual SEI formation taking into account the atomic defect, grain boundary and inhomogeneous growth. **(g)** Calculation of electron tunneling barrier (ΔE_t) by aligning the Fermi level (ε_f), work function (Φ) and band gap (E_g) of the lithium anode and SEI.

Experimental

Lithium bis(trifluoromethane sulfonyl) imide ($LiN(SO_2CF_3)_2$, LiTFSI) (> 98%, TCI) and water (HPLC grade, Sigma-Aldrich) were used as received. Aqueous electrolytes are prepared according to molality (mol-salt in kg-solvent), which were coded by abbreviated concentrations (1 m, 5 m, 10 m, 21 m), with LiTFSI molar fractions being 0.0177 (1m), 0.0826 (5m), 0.1526 (10 m) and 0.2743 (21 m), respectively. The preparation of chevrel phase Mo_6S_8 was decribed previsously, while $LiMn_2O_4$ was purchased from MTI Corporation. Composite electrodes were fabricated by compressing active materials, carbon black, and poly(vinylidene difluoride) (PTFE) at a weight ratio of 8:1:1 onto a stainless steel grid. The full aqueous Li-ion cell was assembled in CR2032-type coin cell using $LiMn_2O_4$ cathode, Mo_6S_8 anode and glass fiber as separator. The cells were cycled galvanostatically on a Land BT2000 battery test system (Wuhan, China). Electrochemical impedance spectroscopy (EIS) was measured on Gamry Interface 1000 (Gamry, USA).

The gas evolution during the formation stage of SEI was quantitatively analyzed with differential electrochemical mass spectrometry (DEMS) and custom-built gas-tight Swagelok^{TM} cells, in which anode (Mo_6S_8), separator, cathode ($LiMn_2O_4$), a stainless steel ring spacer (1 mm in height) and 65 μl of aqueous electrolytes at varying LiTFSI-concentrations were sequentially added. The cell structures and DEMS operation mechanisms have been described previously [17]. To ensure that only the gas generated from the electrochemical reaction be detected, the cells were purged with Ar (~1120 Torr, Research Purity, Matheson Tri-Gas®) overnight, so that any residual gas, either dissolved in electrolytes or adsorbed in cell components, was completely removed. To minimize any

possible water transfer to mass spectrometry, a cold trap was installed at the cell outlet capillaries.

Chemical analysis and depth-profiling of SEI was conducted using time of flight secondary ion mass spectrometry (TOF-SIMS), which is attached on a GAIA Focused Ion Beam and Scanning Electron Microscope. This unique integration of ion mass spectrometry of high sensitivity together with continual FIB etching/sectioning results in a 3D map of mass distribution across the SEI. The depth profiling experiments were performed in static mode where the sputtering gun (Ga^+) was operated over a 4×4 μm^2 area of the electrode surface. Secondary ions were detected in both positive and negative ion mode. TOF-SIMS spectra data were deconvoluted using proprietary TOF-SIMS explorer software.

X-ray photoelectron spectroscopy (XPS) analysis was performed with a high resolution Kratos AXIS 165 X-ray photoelectron spectrometer using monochromic AlKa radiation. All samples were recovered from full aqueous Li-ion cells in 2032 coin cell configuration after repeated cycling to complete SEI formation. The samples were washed by dimethoxyethane (DME) for three times and then dried under vacuum for two hours before entry into XPS chamber. Raman spectra were acquired using Horiba Jobin Yvon Labram Aramis by a 532 nm diode-pumped solid-state laser between 1200 and 100 cm^{-1}. Laser power was set at 150 ~ 450 mV, and 400 scans were accumulated with a resolution of 2 cm^{-1}. All samples were sealed in a test glass tube.

Soft X-ray Absorption Spectroscopy (SXAS) measurements of C, O and F K–edges were performed at beamline 8. 0. 1 of the Advance Light Source (ALS) of Lawrence Berkeley National Laboratory (LBNL). The undulator and spherical grating monochromator supply a

linearly polarized photon beam with resolving power up to 6000. The energy resolution of sXAS is higher than 0.15 eV in this study. All experiments were performed at room temperature, and all spectra were normalized to the beam flux measured by an upstream gold mesh, which is cleaned through in-vacuum Au evaporation especially for C- K and O- K sXAS experiments.

Acknowledgement

CW and KX acknowledge support from DOE ARPA-E (DEAR0000389). LMS acknowledges support from Hundred Talents Program of the Chinese Academy of Sciences. YXL, YQ, and CSW acknowledge the support for the computational work as part of the Nanostructures for Electrical Energy Storage (NEES), an Energy Frontier Research Center funded by the U.S. Department of Energy, Office of Science, Basic Energy Sciences under Award number DESC0001160. JL acknowledges support by NSF ECCS-1610806. This research used resources of the Advanced Light Source, which is a DOE Office of Science User Facility under contract no. DE-AC02-05CH11231.

Reference

(1) Fong, R.; Vonsacken, U.; Dahn, J. R. *Journal of the Electrochemical Society* **1990**, *137*, 2009.

(2) Xu, K. *Chemical Reviews* **2004**, *104*, 4303.

(3) Xu, K. *Chemical Reviews* **2014**, *114*, 11503.

(4) Xu, K.; Lam, Y. F.; Zhang, S. S.; Jow, T. R.; Curtis, T. B. *Journal of Physical Chemistry C* **2007**, *111*, 7411.

(5) Levi, M. D.; Aurbach, D. *Journal of Physical Chemistry B* **1997**, *101*, 4630.

(6) Besenhard, J. O.; Winter, M.; Yang, J.; Biberacher, W. *Journal of Power Sources* **1995**, *54*, 228.

(7) Tasaki, K.; Kanda, K.; Kobayashi, T.; Nakamura, S.; Ue, M. *Journal of the Electrochemical Society* **2006**, *153*, A2192.

(8) Suo, L.; Borodin, O.; Gao, T.; Olguin, M.; Ho, J.; Fan, X.; Luo, C.; Wang, C.; Xu, K. *Science* **2015**, *350*, 938.

(9) Suo, L. M.; Borodin, O.; Sun, W.; Fan, X. L.; Yang, C. Y.; Wang, F.; Gao, T.; Ma, Z. H.; Schroeder, M.; von Cresce, A.; Russell, S. M.; Armand, M.; Angell, A.; Xu, K.; Wang, C. S. *Angewandte Chemie-International Edition* **2016**, *55*, 7136.

(10) Yang, C. Y.; Suo, L. M.; Borodin, O.; Wang, F.; Sun, W.; Gao, T.; Fan, X. L.; Hou, S. Y.; Ma, Z. H.; Amine, K.; Xu, K.; Wang, C. S. *Proceedings of the National Academy of Sciences of the United States of America* **2017**, *114*, 6197.

(11) Suo, L. M.; Han, F. D.; Fan, X. L.; Liu, H. L.; Xu, K.; Wang, C. S. *Journal of Materials Chemistry A* **2016**, *4*, 6639.

(12) Suo, L.; Borodin, O.; Wang, Y.; Rong, X.; Sun, W.; Fan, X.; Xu, S.; Schroeder, M. A.; Cresce, A. V.; Wang, F.; Yang, C.; Hu, Y.-S.; Xu, K.; Wang, C. *Advanced Energy Materials*, 1701189.

(13) Yang, C.; Chen, J.; Qing, T.; Fan, X.; Sun, W.; von Cresce, A.; Ding, M. S.; Borodin, O.; Vatamanu, J.; Schroeder, M. A.; Eidson, N.; Wang, C.; Xu, K. *Joule* **2017**, *1*, 122.

(14) Kim, H.; Hong, J.; Park, K. Y.; Kim, H.; Kim, S. W.; Kang, K. *Chemical Reviews* **2014**, *114*, 11788.

(15) Luo, J. Y.; Cui, W. J.; He, P.; Xia, Y. Y. *Nature Chemistry* **2010**, *2*, 760.

(16) Li, W.; Dahn, J. R.; Wainwright, D. S. *Science* **1994**, *264*, 1115.

(17) McCloskey, B. D.; Bethune, D. S.; Shelby, R. M.; Girishkumar, G.; Luntz, A. C. *Journal of Physical Chemistry Letters* **2011**, *2*, 1161.

(18) Xu, K.; Wang, C. **2016**, *1*, 16161.

(19) Fisher, G. L.; Ohlhausen, J. A.; Wetteland, C. J. *Surface and Interface Analysis* **2005**, *37*, 713.

(20) Wilson, D. J.; Williams, R. L.; Pond, R. C. *Surface and Interface Analysis* **2001**, *31*, 385.

(21) von Cresce, A.; Russell, S. M.; Baker, D. R.; Gaskell, K. J.; Xu, K. *Nano Letters* **2014**, *14*, 1405.

(22) Lu, P.; Harris, S. J. *Electrochemistry Communications* **2011**, *13*, 1035.

(23) McOwen, D. W.; Seo, D. M.; Borodin, O.; Vatamanu, J.; Boyle, P. D.; Henderson, W. A. *Energy & Environmental Science* **2014**, *7*, 416.

(24) Borodin, O.; Suo, L.; Gobet, M.; Ren, X.; Wang, F.; Faraone, A.; Peng, J.; Olguin, M.; Schroeder, M.; Ding, M. S.; Gobrogge, E.; von Wald Cresce, A.; Munoz, S.; Dura, J. A.; Greenbaum, S.; Wang, C.; Xu, K. *ACS Nano* **2017**, *11*, 10462.

(25) Vatamanu, J.; Borodin, O. *J. Phys. Chem. Lett.* **2017**, *8*, 4362.

(26) Jones, J.; Anouti, M.; Caillon-Caravanier, M.; Willmann, P.; Lemordant, D. *Journal of Molecular Liquids* **2010**, *153*, 146.

(27) Smith, A. J.; Burns, J. C.; Zhao, X. M.; Xiong, D. J.; Dahn, J. R. *Journal of the Electrochemical Society* **2011**, *158*, A447.

(28) Smith, A. J.; Burns, J. C.; Dahn, J. R. *Electrochemical and Solid State Letters* **2010**, *13*, A177.

(29) Ploehn, H. J.; Ramadass, P.; White, R. E. *Journal of the Electrochemical Society* **2004**, *151*, A456.

(30) Thomas, M.; Bruce, P. G.; Goodenough, J. B. *Journal of the Electrochemical Society* **1985**, *132*, 1521.

(31) Peled, E. *Journal of the Electrochemical Society* **1979**, *126*, 2047.

(32) Lin, Y. X.; Liu, Z.; Leung, K.; Chen, L. Q.; Lu, P.; Qi, Y. *Journal of Power Sources* **2016**, *309*, 221.

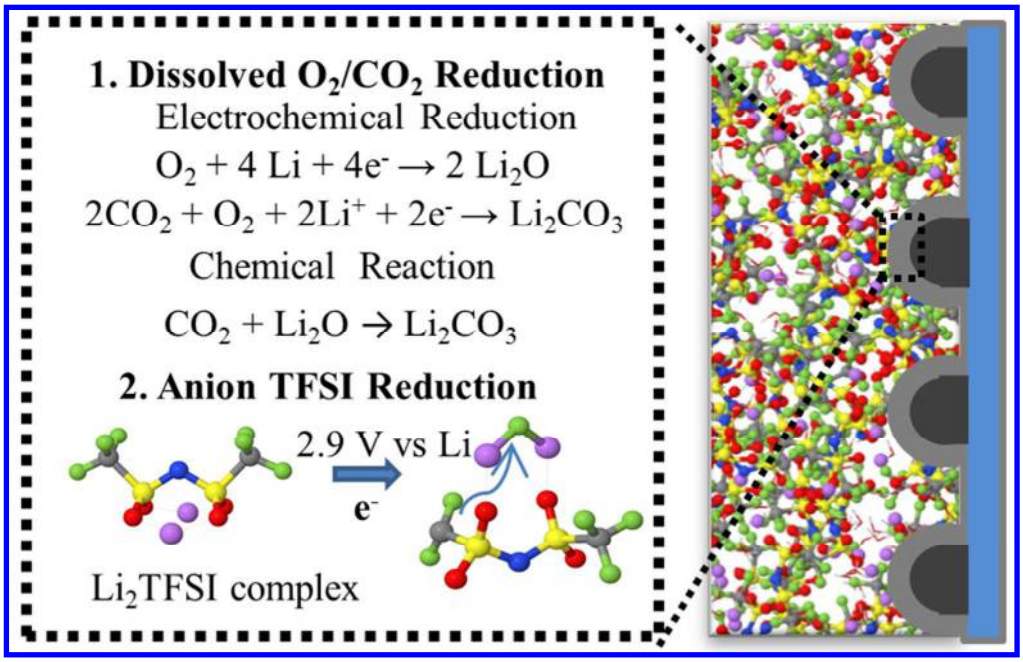

TOC

71x45mm (300 x 300 DPI)